WILEY-VCH

ARTICLE

Highly Active and Easily Fabricated $NiCo_2O_4$ Nanoflowers for Enhanced Methanol Oxidation

Alaa Y. Faid [a,*] and Hadeer Ismail [b]

Abstract Metal oxides with tailored nanomorphology represent a powerful tool to improve the electrocatalytic activity. Herein $NiCo_2O_4$ nanoflowers were synthesized via facile microwave method. $NiCo_2O_4$ nanoflowers were characterized by scanning and transmission electron microscopy, X-ray diffraction (XRD), Raman spectroscopy, N_2 gas adsorption/desorption, and X-ray photoelectron spectroscopy (XPS). Through comparing $NiCo_2O_4$ nanoparticle vs nanoflowers morphology, $NiCo_2O_4$ nanoflowers have a superior mass and specific electroactivity towards oxygen evolution reaction (OER) by achieving a current density of 10 mA/cm^2 at an overpotential of only 280 mV in 1M KOH electrolyte. Moreover, $NiCo_2O_4$ nanoflowers display superior performance for methanol electrooxidation in fuel cells by achieving 200 A/g and recovers 92.3 % of the original activity through the addition of new (1M KOH + 0.5M methanol) electrolyte after 500 cycles.

Introduction

World environmental issues have led to massive research in catalysis for energy devices.[1] Fuel cells represent a green energy conversion devices.[2] Direct methanol fuel cells (DMFCs) operated at low temperatures provide high efficiency and easy refueling characteristics.[3] Noble metals such as Pt are the most active catalyst in DMFCs.[4] However noble metals suffer from limitations such as scarcity, deactivation, and CO poisoning.[4] It is vital to develop and implement a highly active, cheap, and transition metal catalyst for electrooxidation reaction in DMFCs.[5] The research in literature includes doping Pt alloys with another metal, such as Cu or transition metal oxides, such as Co_3O_4, NiO.[6],[7],[8],[9],[10] Transition metal oxides (TMOs) enhance poison tolerance, restrict surface oxidation of catalysts, and improve electrocatalytic alcohol oxidation performance. However, its low conductivity has restricted its application.[11],[12]
Mixed TMOs render rich redox reactions and improve electronic conductivity, which is beneficial to electrochemical applications.[10],[13] Spinel nickel cobaltite ($NiCo_2O_4$) has been widely investigated for potential applications in electromagnetic devices, lithium-ion batteries, water electrolysis, supercapacitors, and sensors due to its abundance, low cost, and environmental friendliness.[14],[15] $NiCo_2O_4$ deduced from the incorporation of Ni atoms into Co_3O_4, provides better electronic conductivity for rapid electron transfer and availability of catalytically active sites.[16],[17] $NiCo_2O_4$ provides a rapid electron transfer from the substituted Ni^{2+} to Co^{3+} in the spinel lattice thus improve methanol electrooxidation activity.[18] Finding an easy and cheap synthesis method able to tailor the $NiCo_2O_4$ morphology is another issue in developing electrocatalyst for large-scale DMFCs applications. Microwave synthesis method has significant benefits of being fast, simple, environmentally–safe, and cheap.[19] The catalyst morphology dramatically impacts the catalytic performance. The catalyst hierarchical morphology can supply high surface roughness, large surface-to-volume ratio. Thus, various nanomorphologies such as wires, plates, rods, spheres, and flowers have been reported.[20],[21] Nanoflower morphology is an effective two-dimensional (2D) structure producing a high surface area,[22] high catalytically active sites, and low electron and ion transport paths resulting in improved catalytic activity.[23],[15]
In this study, a facile and efficient strategy in the synthesis of the hierarchically structured $NiCo_2O_4$ nanoflowers is reported. $NiCo_2O_4$ nanoflowers were characterized using scanning and transmission electron microscopy, Raman spectroscopy, X-ray diffraction (XRD), and X-ray photoelectron spectroscopy (XPS). By comparing the activity of $NiCo_2O_4$ nanoparticles and nanoflowers, $NiCo_2O_4$ nanoflowers show substantially high electrocatalytic methanol oxidation activity and short-term stability.

Results and Discussion

Structural and morphology characterization

Nanoflower morphology growth mechanism is influenced by many factors such as van der Waals forces, hydrogen bonding, electrostatic and dipolar fields. In microwave synthesis, as in Figure 1, hexamethylenetetramine (HMT) hydrolysis helps liberate OH^- ions at high temperature, OH^- ions assist nucleation of NiCo hydroxides. Then, NiCo hydroxides nuclei aggregate due to their high surface energy and thermodynamic instability.[24] As reaction proceeds, the reactants concentration decreases and new particles deposited on formed particles. HMT assists NiCo hydroxides nucleation and form uniform nanoflowers of NiCo hydroxides. NiCo hydroxides are transformed into spinel oxide $NiCo_2O_4$ nanoflower after annealing in an air atmosphere. [24],[25]
Figure 2 displays the morphology and microstructure of $NiCo_2O_4$. Figure 2.a introduces a field emission scanning electron microscopy (FESEM) image $NiCo_2O_4$ nanoparticles while Figure 2.b introduces a (FESEM) image of $NiCo_2O_4$ nanoflowers obtained after annealing of NiCo hydroxide in the air. The annealing process (350 °C for 120 min) introduces minor deterioration of the nanoflowers and $NiCo_2O_4$ preserves the nanoflower morphology.

[a] Alaa Y. Faid
Department of Materials Science and Engineering, Norwegian University of Science and Technology, Trondheim, Norway
alaa.faid@ntnu.no
[b] Hadeer Ismail
Faculty of Engineering, Cairo University

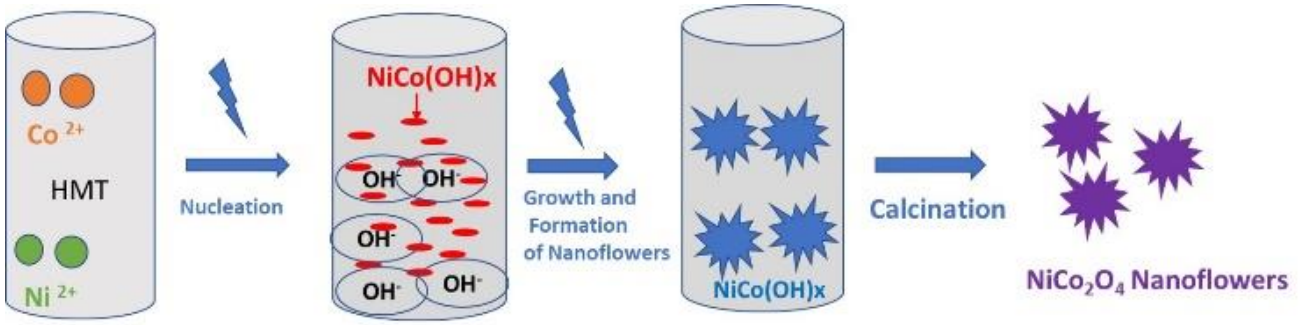

Figure 1. $NiCo_2O_4$ Nanoflower morphology formation mechanism

Figure S1 in the supplementary information (SI) provides more SEM images with various magnifications of $NiCo_2O_4$ nanoflowers. This unique morphology resulted in a large specific surface area (SSA) of $NiCo_2O_4$ (85 m^2/gm), and thus facilitates electrolyte penetration and rapid charge transfer at the electrolyte-electrode interface in $NiCo_2O_4$ nanoflowers surface.[22]

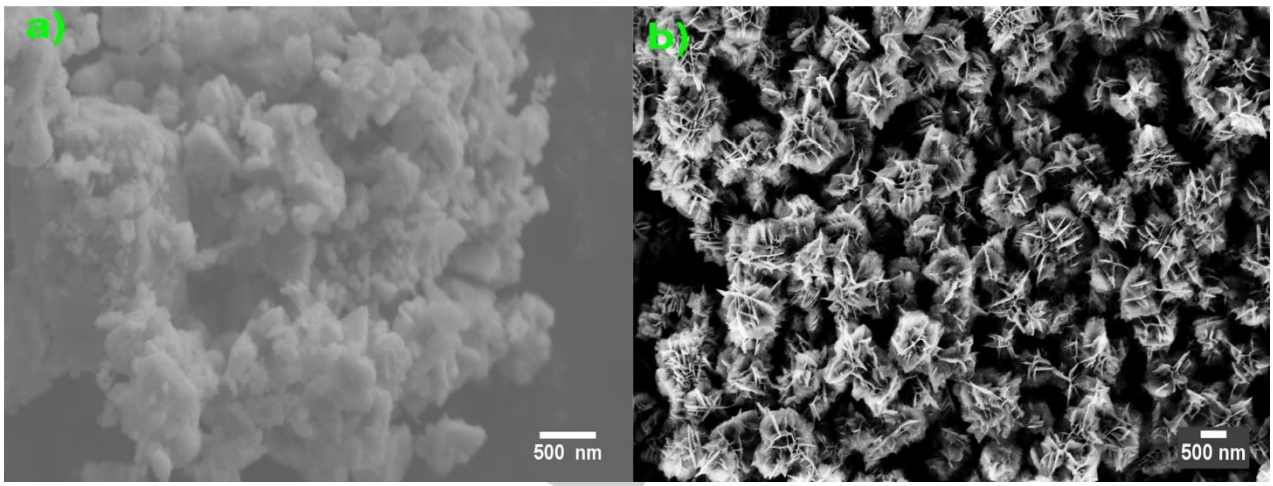

Figure 2. SEM images of a)$NiCo_2O_4$ nanoparticles and b)$NiCo_2O_4$ nanoflower

Figure 3 presents the morphological and structural features of $NiCo_2O_4$ obtained through TEM and selected area diffraction (SAED). Figure 3.a displays the TEM images of the $NiCo_2O_4$ exhibiting nanoflower morphology. As shown in Figure 3.b, The SAED shows a ring pattern, indicating the polycrystalline nature of the $NiCo_2O_4$ nanoflowers.[25],[24]

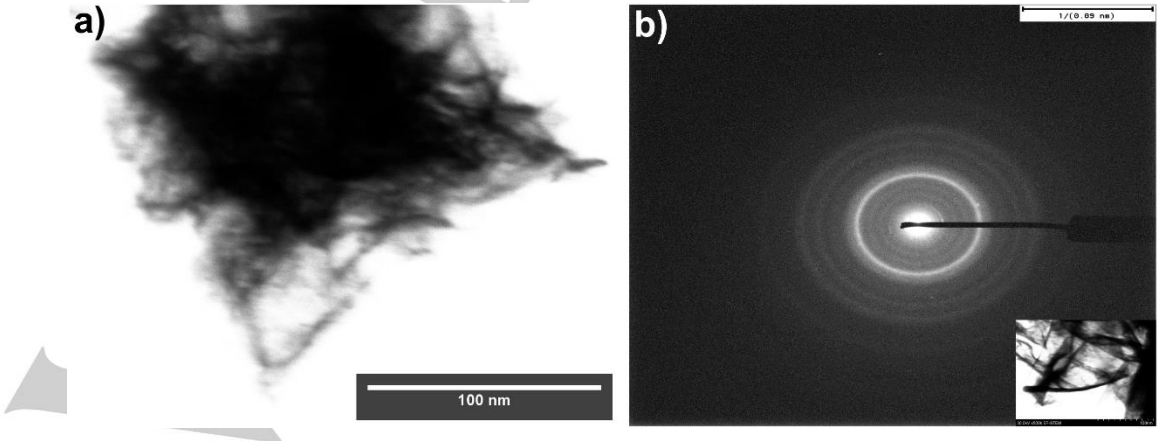

Figure 3. a) STEM images of $NiCo_2O_4$ nanoflowers prepared via microwave process at 450 KX magnification. B) Selected area electron diffraction (SAED) pattern of $NiCo_2O_4$ nanoflowers prepared via microwave process.

$NiCo_2O_4$ nanoflowers were analyzed by XRD to determine their crystallinity and crystallographic structure. Figure 4.a shows XRD pattern of $NiCo_2O_4$ nanoflowers. XRD pattern of $NiCo_2O_4$ nanoflowers shows peaks at a 2θ values of 19°, 31.3°, 36.6°, 44.9°, 59.3°, 65.1°, and 77.4°. These XRD peaks corresponding to the (111), (220), (311), (400), (511), (440), and (533) planes, indicating the cubic spinel crystal structure of $NiCo_2O_4$ (JCPDS card no. 20-0781). No other significant peaks were detected due to the high purity and crystallinity of $NiCo_2O_4$ nanoflowers. [26]

For a further understanding of the composition and structure of these $NiCo_2O_4$ nanoflowers, Raman analysis was carried out to investigate vibrational modes of $NiCo_2O_4$ nanoflowers. The Raman spectrum of the $NiCo_2O_4$ nanoflowers is shown in Figure 4.b. The Raman spectrum display peaks at 473 and 561 cm^{-1}. The peaks at 473 and 561 cm^{-1} correspond to E_g and F_{2g} vibration modes of the $NiCo_2O_4$ nanoflowers, respectively which is related to Co-O and Ni–O vibrations of spinel oxide $NiCo_2O_4$.[27]

Figure 4.c shows N_2 adsorption/ desorption isotherm for $NiCo_2O_4$ nanoflowers. According to IUPAC gas adsorption/ desorption isotherms classification, the N_2 adsorption/ desorption isotherm is of type IV.[28] The BET method allows determination of actual surface area for isotherms of type II or type IV.[28] Hence, the surface area of $NiCo_2O_4$ nanoflowers obtained from BET is noted to be 85 m^2/gm compared to 20 m^2/gm for the nanoparticle morphology. Figure S2 in SI shows pore size distribution of NiCo2O4 nanoflowers and nanoparticles. The pore size distribution was obtained by the Barrett–Joyner–Halenda (BJH) method using the desorption branch of the N_2. The figure S2 shows a broad pore size distribution and most of the pores were in the (2–50 nm) mesoporous-range. [28]

XPS was applied to obtain intensive information on elemental composition, oxidation state, and surface chemistry of $NiCo_2O_4$ nanoflowers. As shown in Figure 5.a, the survey spectrum reveals the presence of Ni, Co, and O elements. Figure 5.b display Nickel Ni 2p spectrum, two spin-orbit peaks appear at about 853.75 eV and 872.65 eV in which corresponds to the Ni $2p_{3/2}$ and Ni $2p_{1/2}$ electronic states, respectively. These two peaks confirming the presence of Ni^{3+} and Ni^{2+} pairs, respectively. The other two broad peaks at approximately 881.3 eV and 862.7 eV correspond to satellite peaks.[17],[29]

Cobalt spectrum is shown in Figure 5.c, two sharp peaks appear at about 781.4 eV and 796.95 eV. These two peaks are assigned to the Co $2p_{3/2}$ and Co $2p_{1/2}$ electronic states, which correspond to Co^{2+} and Co^{3+}, respectively. The other two peaks are shake-up satellites (sat.) peaks. [30],[29] By analyzing the XPS oxygen peak, O1 peak at about 529.8 eV is associated with the metal–oxygen bonds of O–Ni/Co while Ni–OH peak is linked to O_2 peak at 530.4 eV. The peaks 532.2 eV can be assigned to the oxygen ions in surface chemisorbed water.[24] $NiCo_2O_4$ nanoflowers containing the $Co^{3+/2+}$ and $Ni^{3+/2+}$ states provide the synergistic effect of metal ions that allows rapid charge transfer at electrode-interface in methanol electro-oxidation reaction.[31]

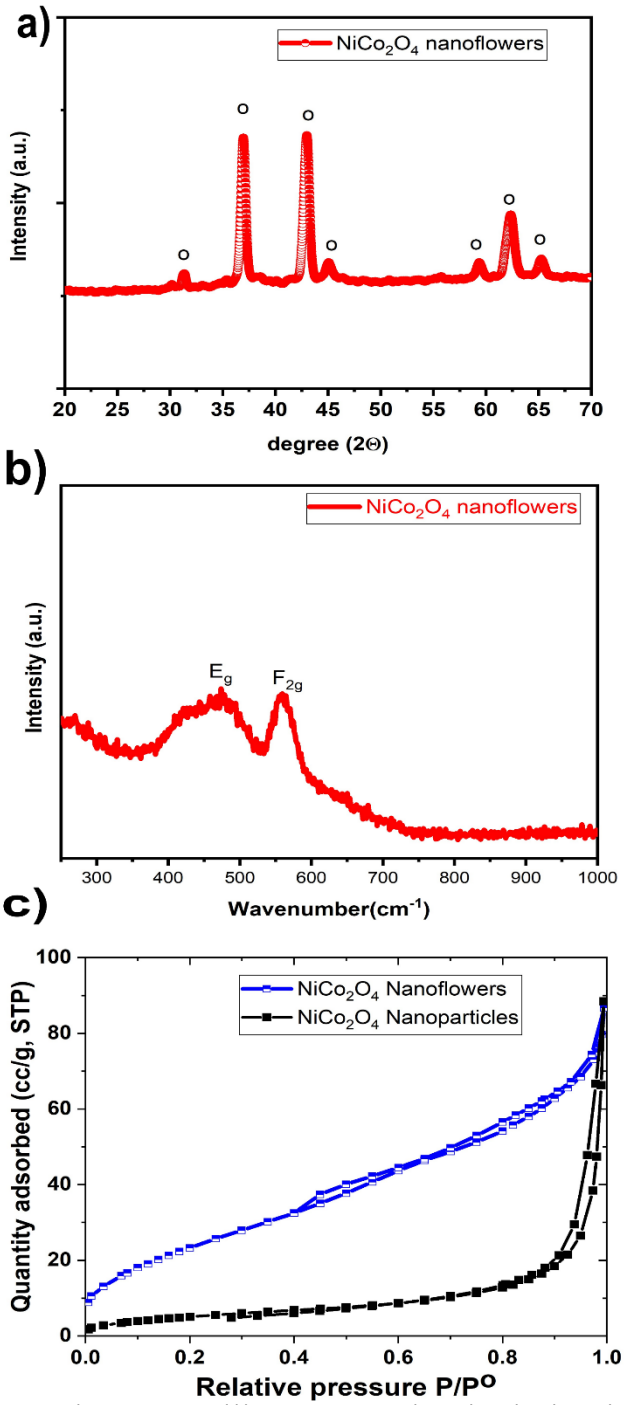

Figure 4. a) XRD pattern and b) Raman spectrum c) N_2 adsorption-desorption isotherms of $NiCo_2O_4$ nanoflowers prepared via microwave process.

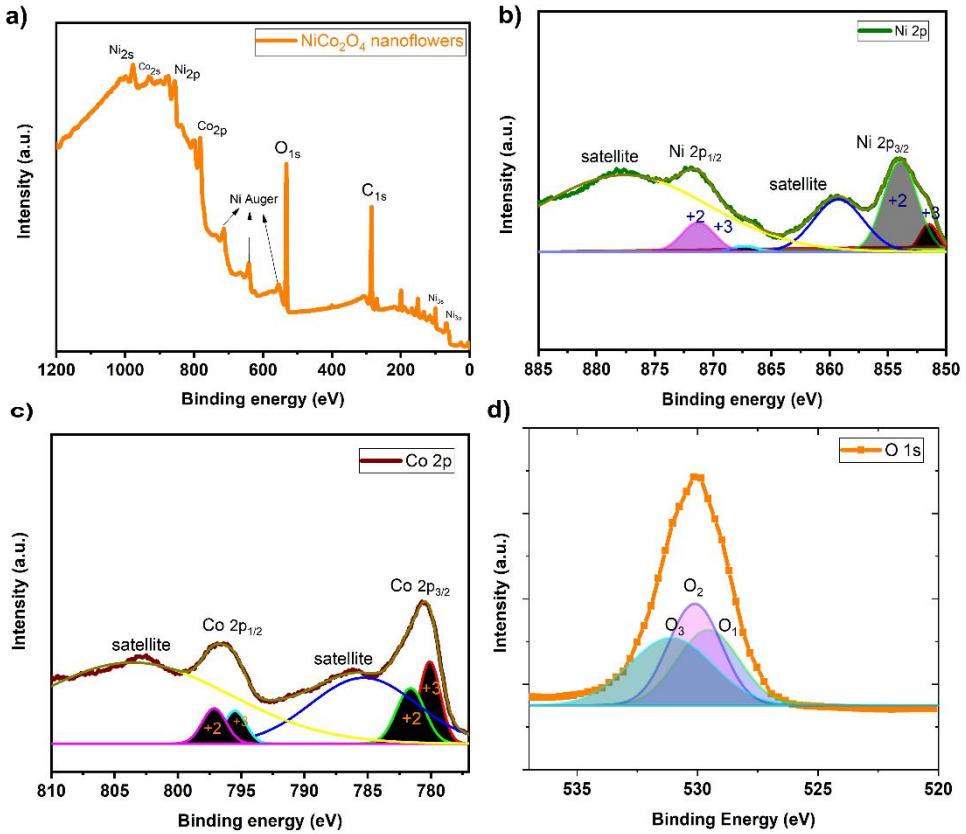

Figure 5. X-ray photoelectron spectrum of $NiCo_2O_4$ nanoflowers prepared via microwave process, a) survey spectrum of $NiCo_2O_4$ nanoflowers, b) Ni 2p peaks, c) Co 2p peaks, and d) O1s peak.

Electrocatalytic characterization

Electrochemical surface area (ECSA) of Ni-based electrodes can be investigated by several methods, using electrochemical double layer capacitance (C_{dl}) or adsorbed hydroxide species. [32] In the method based on adsorbed hydroxide, Ni-based electrocatalyst is initially cathodically polarized for 5 min to eliminate any impurity surface species.[33] As can be seen from Eq. (1):

$$ECSA[cm^2] = \frac{Q[\mu C]}{514\left[\frac{\mu C}{cm^2}\right]} \qquad (1)$$

where Q represents the charge to produce α-Ni $(OH)_2$ during experiments, (514 μC/cm^2) is the theoretical charge required to produce a monolayer of α-Ni$(OH)_2$.[34] Figure 6 represents cyclic voltammetry curves (CVs) of $NiCo_2O_4$ nanoparticle and $NiCo_2O_4$ nanoflowers in the cathodic and anodic regions in N_2-saturated 1M KOH solution. The initial step is the oxidation of metallic nickel to nickel hydroxide (α-Ni $(OH)_2$) at potentials around 0.2 V vs. RHE as in Figure 6.a. By increasing the potential, α-form transform into less hydrated, stable, and irreversible β-Ni$(OH)_2$ phase, which accumulates on Ni surface. β Ni$(OH)_2$ is the predominant surface species in KOH solution, where NiO could be in layers between metallic Ni and β-Ni$(OH)_2$. [35]

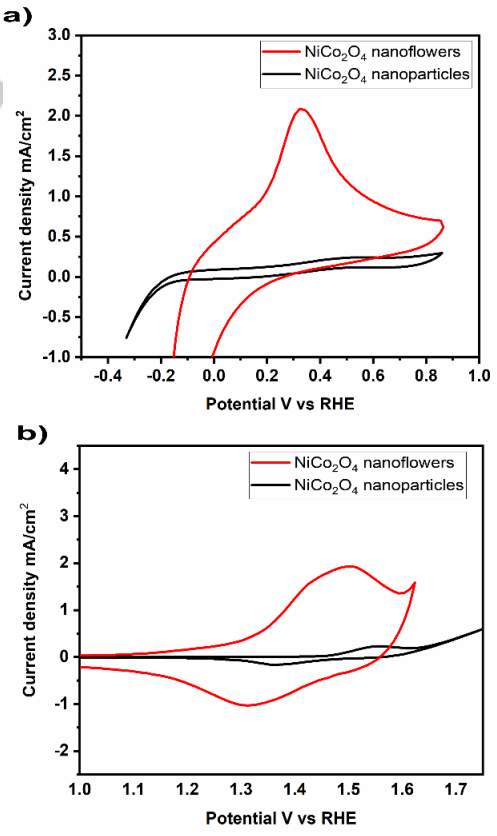

Figure 6. Cyclic voltammograms of a) cathodic and b) anodic of $NiCo_2O_4$ nanoflowers and $NiCo_2O_4$ nanoparticle in 1M KOH at scan rate 5 mV/sec.

ECSA of $NiCo_2O_4$ nanoflowers and $NiCo_2O_4$ nanoparticle were evaluated using the α-$Ni(OH)_2$ peak and Eq (1). An enhancement of ECSA is indicated by a considerable increase in the α-$Ni(OH)_2$ current peak because of enhanced BET surface area. The evaluated ECSA $NiCo_2O_4$ nanoflowers and $NiCo_2O_4$ nanoparticle were 5.1 and 0.3 cm^2, respectively. ECSA based on double layer capacitance (C_{dl}) of CV-scan rate dependence has been carried out in the non-faradaic region and results is presented in Figure S3. The ECSA based on C_{dl} also confirmed the superior electroactivity of nanoflower over nanoparticles morphology. We assumed that ECSA found using this method could be a good estimation of the active surface area of $NiCo_2O_4$ nanoflowers.[36] ECSA was used to compare the electrode performance of $NiCo_2O_4$ nanoparticle and $NiCo_2O_4$ nanoflowers for methanol oxidation. The electrocatalytic performance of $NiCo_2O_4$ nanoflowers toward methanol oxidation reaction (MOR) was investigated. For comparison, the electrocatalytic performance of $NiCo_2O_4$ nanoflowers and commercial $NiCo_2O_4$ nanoparticle control catalysts was measured under similar conditions. All catalysts were loaded on GCE, and catalyst loading was optimized to be 0.5 mg/cm^2. Before the electrocatalytic test, pre-activation was carried out by repetitive CV scans at 5 mV s^{-1} in the potential range of 1.0 –1.7 V vs. reversible hydrogen electrode (RHE) until a steady state CV curve was obtained. Figure 7.a, b, and c display the LSV curves of $NiCo_2O_4$ nanoflowers, Ni nanoparticles, and GCE in 1 M KOH in the absence of 0.5 M methanol electrolyte at 5 mV/sec scan rate. Figure 7.a shows the iR-corrected LSV curves of all samples. GCE bare electrode generates a negligible current density, suggesting that GCE is not catalytically active towards the OER. The overpotential (η_{10}) needed to deliver benchmark current density of 10 mA/ cm^2 is widely used as an indicator to compare the apparent catalytic activity. $NiCo_2O_4$ nanoflowers only need a η_{10} of 280 mV to deliver 10 mA/cm^2, substantially lower than that of $NiCo_2O_4$ nanoparticle. $NiCo_2O_4$ nanoflowers afford superior OER activity by achieving a high current density of 100 mA/cm^2 at η = 370 mV.

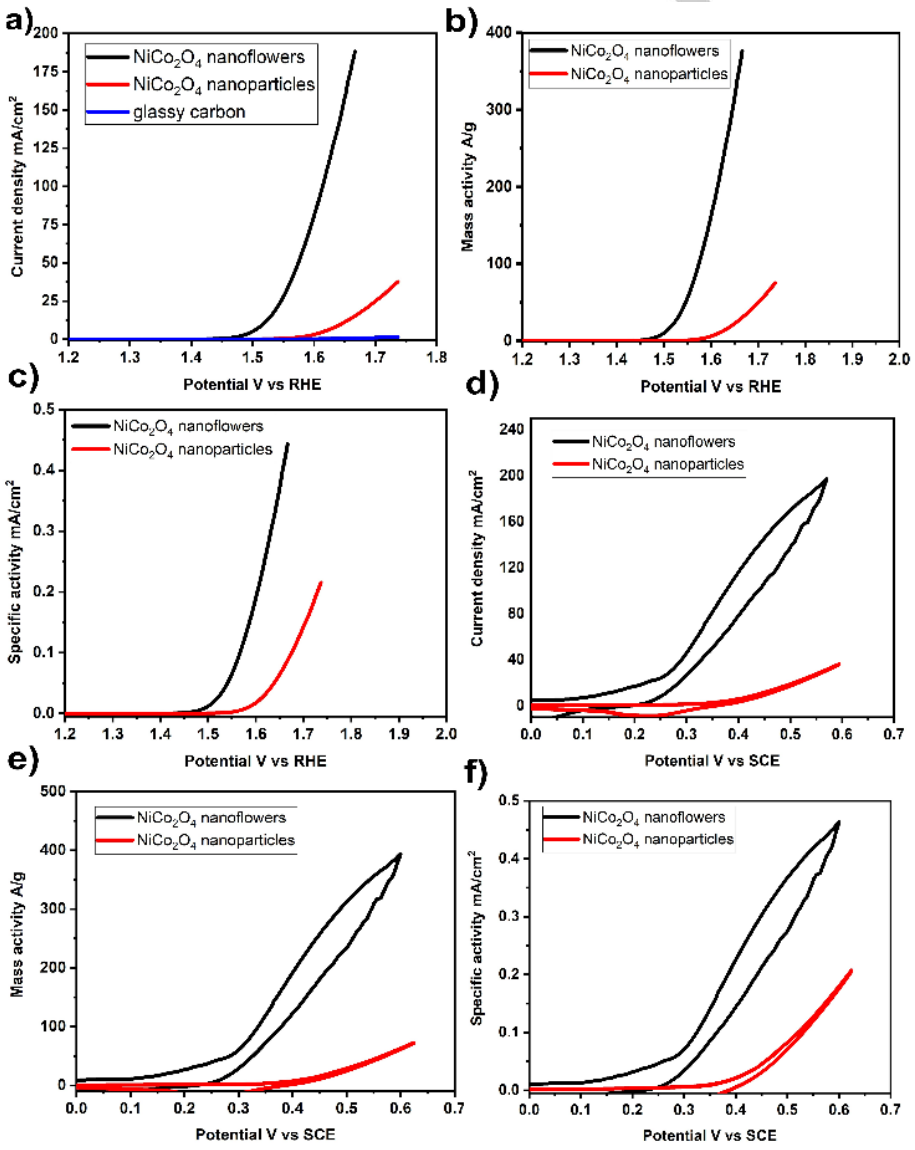

Figure 7. LSV curves $NiCo_2O_4$ nanoparticles and $NiCo_2O_4$ nanoflowers in 1 M KOH normalized to a) geometric surface area b) mass loading c) BET surface area and in 1M KOH/0.5 M methanol normalized to d) geometric surface area e) mass loading f) BET surface area at a scan rate of 5 mV/sec

.

While apparent OER activity is mainly dependent on catalyst loading. Mass and specific activity can better reflect the utilization of catalysts and intrinsic activity of materials.

Mass and specific activity are obtained through normalizing the catalytic current by the mass loading of catalyst and ECSA, respectively. The mass activities of $NiCo_2O_4$ nanoflowers and $NiCo_2O_4$ nanoparticle control catalysts are compared. $NiCo_2O_4$ nanoflowers are found to exhibit a mass activity of 200 A/g at η= 370 mV, substantially higher than those of $NiCo_2O_4$ nanoparticle at the same overpotential. $NiCo_2O_4$ nanoflowers show enhanced specific activity and able to deliver 0.2 mA/cm$^2_{catalyst}$ at η= 370 mV (Figure 7.c), ca.10 times more active than $NiCo_2O_4$ nanoparticles. Therefore it is assumed that high intrinsic (specific) OER activity of $NiCo_2O_4$ nanoflowers results from their unique morphology where more catalytically active sites are exposed, and better mass transport can be achieved. $NiCo_2O_4$ nanoflowers provides an intrinsic activity for OER substantially superior to the literature summarized in Table S1 [37],[38],[39],[40],[41]. Tafel plot is obtained in Figure S4. $NiCo_2O_4$ nanoflowers have a Tafel slope of 50 mV/dec which is lower than obtained for $NiCo_2O_4$ nanoparticles (70 mV/dec) which confirm the rapid OER kinetics for the nanoflower morphology.[42]

The electrocatalytic activity of $NiCo_2O_4$ nanoparticles, and $NiCo_2O_4$ nanoflowers in (1M KOH/0.5M methanol) at 5 mV/sec scan rate were performed and presented in Figure 7.d, 7.e, and 7.f for comparison. $NiCo_2O_4$ nanoflowers exhibit distinctly different behaviors in (1M KOH/0.5M methanol). $NiCo_2O_4$ nanoflowers achieves 100 mA/cm^2 at 415 mV in (1M KOH/0.5M methanol). The mass activity of $NiCo_2O_4$ nanoflowers in (1M KOH/0.5M methanol) is 200 A/g at η = 410 mV. Normalizing methanol oxidation activity to ECSA resulted proves the superior intrinsic activity of $NiCo_2O_4$ nanoflowers towards MOR. The reactions in the alkaline electrolyte can be illustrated as follows: $NiCo_2O_4$ nanoflowers provide rapid charge transfer processes through redox pairs of Co^{2+}/Co^{3+} and Ni^{3+}/Ni^{2+}.[5] These redox couples serve as electroactive centers for methanol electrooxidation. The redox reactions in the alkaline electrolyte are based on the following equations: [12],[43]

$$NiCo_2O_4 + OH^- + H_2O \leftrightarrow NiOOH + 2CoOOH + 2e^- \quad (2)$$

$$CoOOH + OH^- \leftrightarrow CoO_2 + H_2O + e^- \quad (3)$$

$$Ni(OH)_2 + OH^- \leftrightarrow NiOOH + H_2O + e^- \quad (4)$$

As shown in Figure 7, after the addition of 0.5 M methanol into 1 M KOH, the current density increases at 0.3 V due to MOR on $NiCo_2O_4$ nanoflowers. The MOR on $NiCo_2O_4$ nanoflowers electrode can be expressed simply by eqn:[16], [44],[12]

$$2MOOH + 2CH_3OH + {}^5/_2\,O_2 \rightarrow 2M(OH)_2 + 2CO_2 + 3H_2O \quad (5)$$
$$(M = Ni, Co)$$

The onset potential towards MOR of $NiCo_2O_4$ nanoflowers is approximately 0.3 V, which is lower than reported previously for direct electrooxidation of methanol. [45],[44] The superior performance of the $NiCo_2O_4$ nanoflowers electrode is due to rapid charge and electron states between (Co^{2+}/Co^{3+} and Ni^{3+}/Ni^{2+}) in MOR process. [46] The possible mechanism for MOR on $NiCo_2O_4$ nanoflowers are shown in Figure 8.[25] The mechanism of the electro-oxidation of methanol in the nickel-based catalyst is still under debate. However, the Co atom is not shown in Fig. 8 since Co_3O_4 is inactive for methanol oxidation as indicated by many authors[25],[16],[47] MOR requires a large overpotential depending on the catalyst and operating conditions. MOR involves six electrons transfer resulting in slower kinetics on the catalyst.[25] As potential increased, CH_3OH get adsorped, then several dehydrogenates formed on $NiCo_2O_4$ nanoflowers surface and intermediates such as CO_{ads}, and CH_3O produced. CO_{ads} is considered as the primary carbonaceous adsorbate on $NiCo_2O_4$ nanoflowers catalyst surface during methanol oxidation. Therefore, CO* was used as a representative substance in Figure 8. Then COOH intermediate formed at a higher potential. Moreover, unstable COOH will transform into the carbon dioxide product. Finally, carbon dioxide will detach from the surface to recover the catalytic sites.[48]

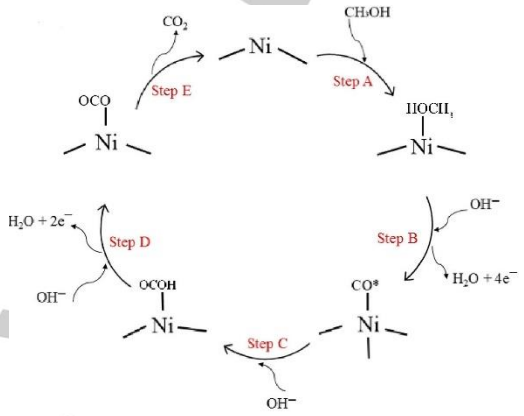

Figure 8. The methanol oxidation reaction (MOR) mechanism on the $NiCo_2O_4$ nanoflowers catalyst surface. [25]

Electrochemical impedance spectroscopy (EIS) is used to investigate electrode-electrolyte interface processes. [49] Figure 9 shows the Nyquist diagrams of $NiCo_2O_4$ nanoparticle and $NiCo_2O_4$ nanoflowers at different potentials in (1M KOH/0.5M methanol). In principle, the charge transfer resistance of electrodes is an important factor that affects catalyst performance.[49] As shown in Figure 9, two main parts are found in the Nyquist diagram: a high-frequency related to the electrolyte and charge transfer resistance and a low-frequency trail from the redox capacitance behavior of nickel and cobalt cations.[50]

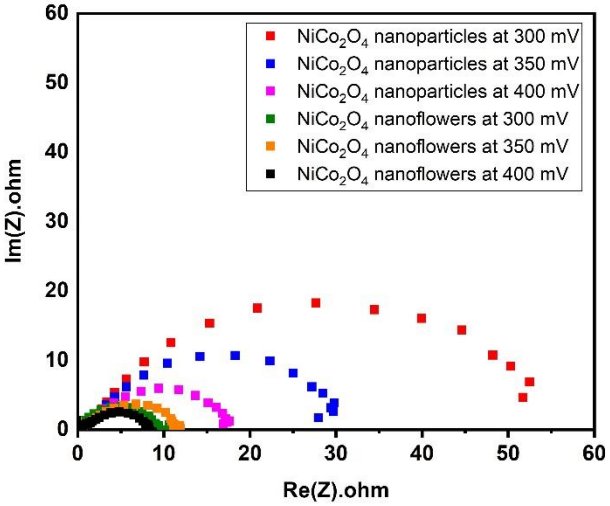

Figure 9. Nyquist plots of EIS in 1M KOH/0.5M methanol: $NiCo_2O_4$ nanoparticle and $NiCo_2O_4$ nanoflowers at different potentials from 300 to 450 mV.

As the potential increases, charge transfer resistance decreases. As expected, the diameters of the semicircle of $NiCo_2O_4$ nanoflowers electrodes were smaller than $NiCo_2O_4$ nanoparticle-modified electrodes, manifesting higher charge transfer rate on

the $NiCo_2O_4$ nanoflowers than on $NiCo_2O_4$ nanoparticle.[51] The lower charge transfer stimulated the electron transfer and enhanced adsorption of reactants on the $NiCo_2O_4$ nanoflowers, revealing the high intermediate poisoning tolerance of $NiCo_2O_4$ nanoflowers. In the MOR, CH_3OH produces the intermediates after the complex procedures of the adsorption and several dehydrogenations on $NiCo_2O_4$ nanoflowers.[10],[24],[52],[49] The diameters of the semicircles are observed to decrease with the increase in applied potential due to an increase in the charge transfer kinetics during MOR and are shown in Figure 9. This observation supports the improved charge transfer kinetics to the adsorbed reactant ions and that facilitates MOR reaction for nanoflowers than nanoparticles.[53],[24]

Chronoamperometry (CA) represents an important technique for characterization and investigation of electrochemical stability of the catalyst during methanol oxidation.[54] According to the discussion above, 0.35 V was selected as the optimal potential for the CA tests and carried out for 1000 s. Figure 10.a shows the stability of $NiCo_2O_4$ nanoflowers and $NiCo_2O_4$ nanoparticle during MOR. $NiCo_2O_4$ nanoflowers displays promising stability in 1000 s. A minor current decay for $NiCo_2O_4$ nanoflowers occurs during initial stage due to oxidation intermediate poisoning. However, $NiCo_2O_4$ nanoflowers proves superior stability during MOR as it did not show any noticeable deterioration after 1000 sec.

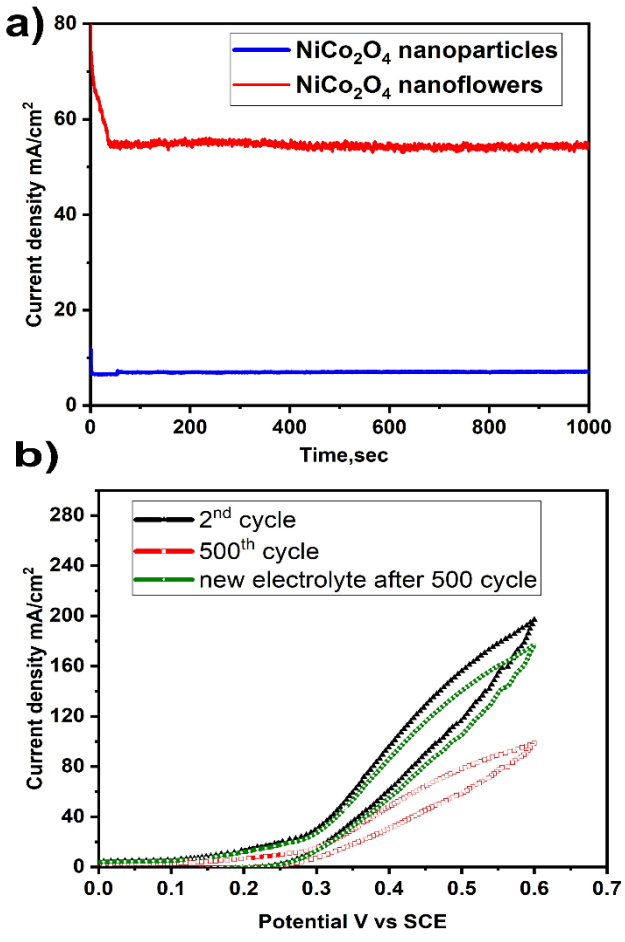

Figure 10. a) Chronoamperometry (CA) curves of $NiCo_2O_4$ nanoparticle and $NiCo_2O_4$ nanoflowers in (1M KOH/0.5M methanol) at 0.35 V (for 1000 s); (b) Cyclic voltammetry (CV) curves of $NiCo_2O_4$ nanoflowers measured at different cycles in (1M KOH/0.5M methanol) at a 5 mV/sec scan rate.

The current density of $NiCo_2O_4$ nanoflowers obtained from CA is in good compromise with the current density obtained from CV (Figure 7.a). Cyclic voltammetry (CV) is another factor in assessing the stability of the catalyst, the CV curves in Figure 10.b show that $NiCo_2O_4$ nanoflowers maintains a current density of 55.1% of its original value after 500 cycles at 5 mV/sec scan rate. Furthermore, by exchanging with a new electrolyte solution, the current density of $NiCo_2O_4$ nanoflowers at 0.6 V preserves 92.3% of the original value.

$NiCo_2O_4$ nanoflowers show substantial activity compared to the literature summarized in Table S2.[16],[12],[55] $NiCo_2O_4$ nanoflowers exhibit a superior activity and stability towards methanol electrooxidation, which resulted from synergistic effects of nickel and cobalt faradaic redox reaction, unique nanoflower morphology and shorter diffusion path which is required for DMFCs anodic materials.[13] There are two mechanisms to reduce CO poisoning: 1) electronic effect: low CO adsorption energy which associated with local electron density moving away from the metal surface and alters the potential and decomposition kinetics. This phenomenon provides facile desorption of CO and reaction equilibrium between CO and oxidants to reduce CO poisoning, 2) bifunctional effect: CO oxidative removal using the coadsorbed hydroxyl ion (OH^-) of the neighboring metal which leads to oxidation of the adsorbed CO on catalyst surface to carbon dioxide (CO_2). [56] Recently, DFT studies carried out by Xun et al. show that CH_3OH prefers to bind on Ni, whereas CO prefers to bind on Co than Ni, thus the coexistence of Ni and Co in the catalysts system would reduce the overall poisoning effect in the catalyst.[56],[48] [25],[24],[54] Accordingly, $NiCo_2O_4$ nanoflowers have high activity and stability towards methanol oxidation.

Conclusions

$NiCo_2O_4$ nanoflowers was prepared through a facile microwave-assisted synthesis process. Detailed structural and electrochemical characterization has been carried out. The electrochemical activity of $NiCo_2O_4$ nanoflowers towards methanol oxidation was studied. $NiCo_2O_4$ nanoflowers showed high electrocatalytic activity and excellent short-term stability compared to $NiCo_2O_4$ nanoparticles. The superior performance of $NiCo_2O_4$ nanoflowers is due to its hierarchical nanoflower morphology and high surface area.

Supporting Information Summary

Supporting information contains details of experimental methods, SEM images with different magnifications of $NiCo_2O_4$ nanoflowers. The pore size distribution of $NiCo_2O_4$ nanoflowers and nanoparticles, ECSA determination using CV-scan rate dependence. Tafel plot of $NiCo_2O_4$ nanoflowers and nanoparticles during OER reaction. Table S1 comparing $NiCo_2O_4$ nanoflowers OER activity with reported literature in alkaline electrolytes, Table S2: Nickel cobalt catalyst MOR activity comparison in (1M KOH/0.5 M methanol) electrolyte.

Acknowledgments

Erasmus Mundus scholarship is acknowledged for making this work available.

Keywords: Methanol Oxidation • Microwave • Nanoflowers • $NiCo_2O_4$ •

[1] M. Shao, *Catalysts* **2015**, *5*, 2115.

[2] L. Carrette, K. A. Friedrich, U. Stimming, *ChemPhysChem* **2000**, *1*, 162.

[3] B. C. Ong, S. K. Kamarudin, S. Basri, *Int. J. Hydrogen Energy* **2017**, *42*, 10142.

[4] B. Zhang, Y. Niu, J. Xu, X. Pan, C.-M. Chen, W. Shi, M.-G. Willinger, R. Schlögl, D. S. Su, *Chem. Commun.* **2016**, *52*, 3927.

[5] M. Yu, J. Chen, J. Liu, S. Li, Y. Ma, J. Zhang, J. An, *Electrochim. Acta* **2015**, *151*, 99.

[6] L. Zhang, X.-F. Zhang, X.-L. Chen, A.-J. Wang, D.-M. Han, Z.-G. Wang, J.-J. Feng, *J. Colloid Interface Sci.* **2019**, *536*, 556.

[7] Y.-C. Shi, L.-P. Mei, A.-J. Wang, T. Yuan, S.-S. Chen, J.-J. Feng, *J. Colloid Interface Sci.* **2017**, *504*, 363.

[8] X.-W. Xie, J.-J. Lv, L. Liu, A.-J. Wang, J.-J. Feng, Q.-Q. Xu, *Int. J. Hydrogen Energy* **2017**, *42*, 2104.

[9] Y. Liu, Y. Huang, Y. Xie, Z. Yang, H. Huang, Q. Zhou, *Chem. Eng. J.* **2012**, *197*, 80.

[10] L. Zhang, D. Zhang, Z. Ren, M. Huo, G. Dang, F. Min, Q. Zhang, J. Xie, *ChemElectroChem* **2017**, *4*, 441.

[11] N. Spinner, W. E. Mustain, *Electrochim. Acta* **2011**, *56*, 5656.

[12] W. Wang, Q. Chu, Y. Zhang, W. Zhu, X. Wang, X. Liu, *New J. Chem.* **2015**, *39*, 6491.

[13] L. Qian, L. Gu, L. Yang, H. Yuan, D. Xiao, *Nanoscale* **2013**, *5*, 7388.

[14] A. Y. Faid, A. O. Barnett, F. Seland, S. Sunde, *J. Electrochem. Soc.* **2019**, *166*, F519.

[15] A. Faid, A. Oyarce Barnett, F. Seland, S. Sunde, A. Y. Faid, A. Oyarce Barnett, F. Seland, S. Sunde, *Catalysts* **2018**, *8*, 614.

[16] A. K. Das, R. K. Layek, N. H. Kim, D. Jung, J. H. Lee, *Nanoscale* **2014**, *6*, 10657.

[17] J. F. Marco, J. R. Gancedo, M. Gracia, J. L. Gautier, E. Ríos, F. J. Berry, *J. Solid State Chem.* **2000**, *153*, 74.

[18] E. Umeshbabu, G. Ranga Rao, *Electrochim. Acta* **2016**, *213*, 717.

[19] I. Bilecka, M. Niederberger, *Nanoscale* **2010**, *2*, 1358.

[20] W. A. Abbas, M. Ramadan, A. Y. Faid, A. M. Abdellah, A. Ouf, N. Moustafa, N. K. Allam, *Environ. Nanotechnology, Monit. Manag.* **2018**, *10*, 87.

[21] A. Y. Faid, N. K. Allam, *RSC Adv.* **2016**, *6*, 80221.

[22] J. Mu, J. Li, E. Yang, X. Zhao, *ACS Appl. Energy Mater.* **2018**, *1*, 3742.

[23] M. Ledendecker, G. Clavel, M. Antonietti, M. Shalom, *Adv. Funct. Mater.* **2015**, *25*, 393.

[24] B. Wang, Y. Cao, Y. Chen, R. Wang, X. Wang, X. Lai, C. Xiao, J. Tu, S. Ding, *Inorg. Chem. Front.* **2018**, *5*, 172.

[25] H. Gao, Y. Cao, Y. Chen, X. Lai, S. Ding, J. Tu, J. Qi, *J. Alloys Compd.* **2018**, *732*, 460.

[26] D. Chanda, J. Hnát, T. Bystron, M. Paidar, K. Bouzek, *J. Power Sources* **2017**, *347*, 247.

[27] M. N. Iliev, P. Silwal, B. Loukya, R. Datta, D. H. Kim, N. D. Todorov, N. Pachauri, A. Gupta, *J. Appl. Phys.* **2013**, *114*, 0.

[28] K. S. W. Sing, *Pure Appl. Chem.* **2007**, *57*, 603.

[29] C. Mahala, M. Basu, *ACS Omega* **2017**, *2*, 7559.

[30] J. F. Marco, J. R. Gancedo, M. Gracia, J. L. Gautier, E. Ríos, F. J. Berry, *J. Solid State Chem.* **2000**, *153*, 74.

[31] A. R. Jadhav, H. A. Bandal, A. A. Chaugule, H. Kim, *Electrochim. Acta* **2017**, *240*, 277.

[32] D. S. Hall, C. Bock, B. R. MacDougall, *J. Electrochem. Soc.* **2014**, *161*, H787.

[33] M. Alsabet, M. Grden, G. Jerkiewicz, *Electrocatalysis* **2014**, *5*, 136.

[34] M. Alsabet, M. Grden, G. Jerkiewicz, *Electrocatalysis* **2011**, *2*, 317.

[35] M. Alsabet, M. Grdeń, G. Jerkiewicz, *Electrocatalysis* **2014**, *6*, 60.

[36] D. S. Hall, C. Bock, B. R. MacDougall, *J. Electrochem. Soc.* **2013**, *160*, F235.

[37] J. Chang, Y. Xiao, M. Xiao, J. Ge, C. Liu, W. Xing, *ACS Catal.* **2015**, *5*, 6874.

[38] D. Xiong, X. Wang, W. Li, L. Liu, *Chem. Commun.* **2016**, *52*, 8711.

[39] Z. Yin, C. Zhu, C. Li, S. Zhang, X. Zhang, Y. Chen, *Nanoscale* **2016**, *8*, 19129.

[40] S. Barwe, C. Andronescu, E. Vasile, J. Masa, W. Schuhmann, *Electrochem. commun.* **2017**, *79*, 41.

[41] X. Zhang, L. Huang, Q. Wang, S. Dong, *J. Mater. Chem. A* **2017**, *5*, 18839.

[42] T. Shinagawa, A. T. Garcia-Esparza, K. Takanabe, *Sci. Rep.* **2015**, *5*, 1.

[43] M. Silambarasan, P. S. Ramesh, D. Geetha, *J. Mater. Sci. Mater. Electron.* **2017**, *28*, 323.

[44] G. Chen, Y. Gao, H. Zhang, *RSC Adv.* **2016**, *6*, 30488.

[45] M. Asgari, M. G. Maragheh, R. Davarkhah, E. Lohrasbi, A. N. Golikand, *Electrochim. Acta* **2012**, *59*, 284.

[46] M. U. A. Prathap, B. Satpati, R. Srivastava, *Electrochim. Acta* **2014**, *130*, 368.

[47] M. U. Anu Prathap, R. Srivastava, *Nano Energy* **2013**, *2*, 1046.

[48] X. Cui, W. Guo, M. Zhou, Y. Yang, Y. Li, P. Xiao, Y. Zhang, X. Zhang, *ACS Appl. Mater. Interfaces* **2015**, *7*, 493.

[49] D. Chakraborty, I. Chorkendorff, T. Johannessen, *J. Power Sources* **2006**, *162*, 1010.

[50] W. Huang, Y. Cao, Y. Chen, J. Peng, X. Lai, J. Tu, *Appl. Surf. Sci.* **2017**, *396*, 804.

[51] T.-H. Ko, S. Radhakrishnan, M.-K. Seo, M.-S. Khil, H.-Y. Kim, B.-S. Kim, *J. Alloys Compd.* **2017**, *696*, 193.

[52] L. Gu, L. Qian, Y. Lei, Y. Wang, J. Li, H. Yuan, D. Xiao, *J. Power Sources* **2014**, *261*, 317.

[53] J. Xu, Y. Liu, J. Li, I. Amorim, B. Zhang, D. Xiong, N. Zhang, S. M. Thalluri, J. P. S. Sousa, L. Liu, *J. Mater. Chem. A* **2018**, *6*, 20646.

[54] V. L. Oliveira, C. Morais, K. Servat, T. W. Napporn, G. Tremiliosi-Filho, K. B. Kokoh, *Electrochim. Acta* **2014**, *117*, 255.

[55] R. Ding, L. Qi, M. Jia, H. Wang, *J. Power Sources* **2014**, *251*, 287.

[56] R. P. Antony, A. K. Satpati, B. N. Jagatap, *ChemElectroChem* **2017**, *4*, 2989.

Entry for the Table of Contents (Please choose one layout)

Layout 2:

ARTICLE

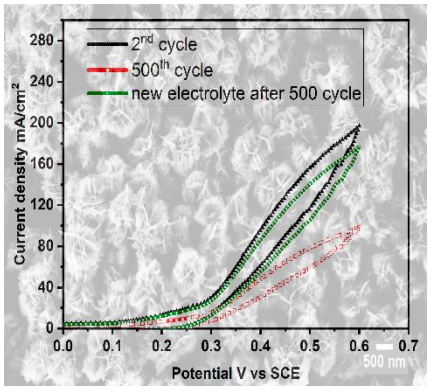

Alaa Y Faid [1,] and Hadeer Ismail [2]*

Page 1 – Page 9.

Highly Active and Easily Fabricated $NiCo_2O_4$ Nanoflowers for Enhanced Methanol Oxidation

Fuel cells represent the green future of energy conversion devices. Focusing on activity-cost issue, $NiCo_2O_4$ catalyst was synthesized and investigated as a catalyst for methanol oxidation. By comparing nanoparticle vs nanoflowers morphology, $NiCo_2O_4$ nanoflowers achieving 200 Ag^{-1} and recovers 92.3 % of the original activity through the addition of new (1M KOH + 0.5 M methanol) electrolyte after 500 cycles. $NiCo_2O_4$ nanoflowers represent a cheap and active catalyst for methanol oxidation in direct methanol fuel cells.